Conductance of a quantum wire with a Gaussian impurity potential and variable cross-sectional shape

Vassilios Vargiamidis* and Hariton M. Polatoglou
Department of Physics, Aristotle University, GR-54124 Thessaloniki, Greece
(Received 19 July 2004; revised manuscript received 12 November 2004; published 2 February 2005)

We calculate the conductance through a Gaussian impurity potential in a quantum wire using the Lippmann-Schwinger equation. The impurity has a decay length d along the propagation direction while it is localized along the transverse direction. In the case of a repulsive Gaussian impurity it is shown that the conductance quantization is strongly affected by the decay length. In particular, increasing d causes gradual suppression of backscattering and smaller contribution of evanescent modes, leading to progressively sharper conductance steps. The dependence of the conductance on the impurity position is also examined. In the case of an attractive Gaussian impurity it is shown that multiple quasibound states are formed due to the finite size of the impurity. By varying the size of the impurity these quasibound states may evolve into highly localized states with greatly enhanced lifetime. It is also shown (for a model impurity potential very similar to the Gaussian) that the transmission exhibits asymmetric Fano line shape. Under certain circumstances the Fano line shape may appear "inverted" or evolve into a Breit-Wigner dip. We consider also the effects of the cross-sectional shape of the wire on the quantum transmission. It is shown that varying the cross-sectional shape causes shifting of the positions of the conductance steps (which is due to the rearrangement of the transverse energy levels) and influences the character of conductance quantization.

DOI: 10.1103/PhysRevB.71.075301 PACS number(s): 72.10.Fk, 73.63.Nm

I. INTRODUCTION

Since the discovery of the quantized conductance,[1,2] of electron transport through narrow wires, much effort has been devoted to the description of electron scattering from impurities in such systems.[3–23] In most of these scattering calculations the impurity potential is taken to be the idealized model of the Dirac δ function. The model of the δ-function scatterer is used mainly for two reasons. First, it allows in most cases for an analytical solution of the scattering problem with a relatively small amount of effort, and second, it captures the basic physics of the problem under consideration.

Although sometimes useful, the use of a δ function scatterer in an infinite rectilinear quantum wire causes some problems. One such problem is the divergence of the quasibound states[20,24] as the number of transverse modes increases. Moreover, it has been proved[22,23] that a δ-function impurity in a quantum wire scatters no electrons if the number of evanescent modes is extended towards infinity. This leads to perfect transmission for all values of the Fermi energy and not just at channel threshold (which occurs when a finite number of modes is kept). In addition the δ-function potential is quite rough and irregular, whereas any realistic model of an impurity should have a smoother potential and finite range.

Several works[8,12,18,24] have discussed the case of an impurity that has a lateral extension but is a δ function along the propagation direction of a rectilinear quantum wire. For this slightly more realistic and analytically solvable model of an impurity potential (for which the problem of the divergence of the quasibound states is removed) the conductance shows no drastic change[24] compared to the conductance through a pure δ-function impurity in the wire. The case where the impurity is represented by a rectangular barrier or attractive square well along the propagation direction has been examined in Refs. 6 and 19. However, a more realistic model for the potential of an impurity in a quantum wire should have a finite range with some decay length (that is, an impurity with a smooth potential profile) along the propagation direction. One important issue therefore is how an impurity of this type affects the conductance of a rectilinear quantum wire. In this case an analytical solution to the scattering problem is not possible and a numerical approach is required.

Another important issue related to electron transmission through an impurity in a three-dimensional (3D) quantum wire is how the geometry of the wire (that is, the shape of the transverse cross section) affects the conductance. This issue has been investigated in the case of 3D quantum constrictions without impurities in the presence[25] and absence[16,26] of a magnetic field. In addition it has also been discussed in the case of a quantum wire with a δ function impurity in the presence[23] and absence [27] of a magnetic field. One of the main results of these investigations is that the conductance of a quantum constriction[16,25,26] as well as the conductance of a quantum wire with a δ function impurity[23,27] is determined not only by the cross-sectional area but also by the shape of the cross section.

The purpose of this paper is twofold. The first objective is to present a brief description of our numerical method for solving the Lippmann-Schwinger equation[28] (LSE) for a general finite-size impurity in a rectilinear quantum wire. We then apply this method in the case of a Gaussian impurity potential with a decay length d along the propagation direction. For the shake of clarity we make the simplifying assumption that the impurity is localized along the transverse direction. We find that as d increases the contribution of the

evanescent (tunneling) modes becomes negligible and the backscattering is suppressed resulting to conductance with progressively sharper quantum steps. We also show that varying the transverse position of the impurity leads to shifting of the energy subbands (in the scattering region) and may strongly affect the quantization of the conductance steps. In the case of an attractive Gaussian impurity we show that there exist multiple resonance dips in the conductance which are due to the formation of discrete levels in the continuum and their interaction with the continuum states. We examine the behavior of a resonance dip location E_{res} (at which the conductance drops to zero) and also the behavior of the resonance half width Γ with increasing values of the decay length of the impurity. We show that E_{res} as a function of the decay length decreases and for some appropriate values of d the half width Γ shrinks to infinitesimally small value which corresponds to a very stable state with greatly enhanced lifetime. We also examine the transmission through a second-type attractive impurity potential which is very similar to the Gaussian but having also a lateral extension. We find that an asymmetric Fano resonance appears in the transmission versus Fermi energy which (for large enough values of the decay length) transforms into a Breit-Wigner dip. For certain values of the decay length and the intrasubband coupling matrix element the resonance energy coincides with the energy of the transmission zero, leading to a completely symmetric dip. Also for certain ranges of the above parameters the Fano resonance is "inverted."

The second objective is to extend our previous calculations[23,27] and investigate shape effects of the cross section of a 3D quantum wire on the conductance through a Gaussian impurity. We find that increasing the cross-sectional shape anisotropy (keeping the cross-sectional area fixed) causes shifting of the positions of the conductance steps, which is due to the rearrangement of the transverse energy levels. Further, by varying the shape of the cross section, symmetry or accidental degeneracies may cause the disappearance of some steps, resulting in step heights of $2(2e^2/h)$.

For an arbitrary shape of the impurity potential an analytical solution of the LSE is not possible. The simple numerical method we developed in order to solve the LSE can be used for calculating the conductance of a quantum wire with an arbitrary impurity potential. It can also be used in the case of multiple scattering centers of arbitrary shape by treating them as a large composite scatterer.

The paper is organized as follows. In Sec. II we describe the theoretical method and the numerical solution of the LSE for obtaining the transmission amplitudes and conductance of the wire. In Sec. III we investigate the effects of the impurity on the conductance. In Sec. IV we analyze the effects of the shape of the cross section of the quantum wire on electron transmission through the impurity and we present a brief summary of our results in Sec. V.

II. THEORETICAL FORMULATION

We consider an infinitely long two-dimensional (2D) rectilinear quantum wire in which electrons are confined along the y direction (transverse direction) but are free to move along the x direction (propagation direction). The cross section is uniform along the wire. The Hamiltonian can be written as

$$H = H_0 + V_i, \tag{1}$$

where $V_i = V_i(x,y)$ is the scattering potential of any defects or impurities in the wire. The unperturbed Hamiltonian H_0 is given as the sum of the kinetic energy plus the confining potential $V_c(y)$, i.e.,

$$H_0 = \frac{\mathbf{p}^2}{2m^*} + V_c(y), \tag{2}$$

where m^* is the effective mass of the electron.

The energy eigenstates of the unperturbed wire—i.e., of H_0—are given as

$$\psi_{\mathbf{p}}^{(0)}(x,y) = \frac{1}{\sqrt{2\pi\hbar}} e^{ip_x x/\hbar} \phi_n(y), \tag{3}$$

where $\phi_n(y)$ are the normal confinement modes (quantum channels) of the wire. The energy eigenvalues of H_0 are $E = (p_x^2/2m^*) + E_n$, where $p_x = \hbar k_x$ has a continuous spectrum, n are subband indices, and E_n are the subband energies.

In the presence of the scattering potential V_i we must solve the following Schrödinger equation:

$$(H_0 + V_i)|\psi\rangle = E|\psi\rangle. \tag{4}$$

Equation (4) has the solution

$$|\psi_{\mathbf{p}}^{(+)}\rangle = |\psi_{\mathbf{p}}^{(0)}\rangle + \frac{1}{E - H_0 + i\varepsilon} V_i |\psi_{\mathbf{p}}^{(+)}\rangle, \tag{5}$$

which is the LSE of scattering theory. This solution corresponds to the incident wave on the scatterer plus an outgoing wave traveling away from the scatterer. Assuming a finite-range and local scattering potential, Eq. (5) can be written in the position basis as an integral equation for scattering,

$$\psi_{\mathbf{p}}^{(+)}(x,y) = \psi_{\mathbf{p}}^{(0)}(x,y) + \frac{2m}{\hbar^2} \int_{-\infty}^{\infty} dx' \int_{-\infty}^{\infty} dy' G^{(0)}(x,y;x',y') \times V_i(x',y') \psi_{\mathbf{p}}^{(+)}(x',y'), \tag{6}$$

where $G^{(0)}(x,y;x',y')$ is the retarded Green's function (which is energy dependent) of the unperturbed wire and takes the form[29]

$$G^{(0)}(x,y;x',y') = \sum_{n'=1}^{\infty} \phi_{n'}(y) \phi_{n'}^*(y') \frac{e^{ik_{n'}|x-x'|}}{2ik_{n'}}. \tag{7}$$

The wave vectors for the propagating modes are $k_{n'} = [2m^*(E - E_{n'})]^{1/2}/\hbar$. The wave vectors for the evanescent modes are obtained by setting $k_{n'} = i\kappa_{n'}$. The scattered modes n' in the Green's function of Eq. (7) are propagating or evanescent depending on whether $E_{n'}$ is less or greater than the Fermi energy E.

The above procedure applies to a general finite-range scattering potential V_i. For a particular form of the potential V_i, the solution to the integral equation (6) for the unknown

wave function $\psi_{\mathbf{p}}^{(+)}(x,y)$ will enable us to extract the current transmission amplitudes. However, since the unknown wave function $\psi_{\mathbf{p}}^{(+)}(x,y)$ appears also under the integral the solution to Eq. (6) (valid throughout the whole wire) requires first finding the wave function in the scattering region, i.e., in the region where $V_i(x,y) \neq 0$.

We consider now electron scattering from an impurity potential of the form

$$V_i(x,y) = \frac{\hbar^2 \gamma}{2m^*} \delta(y - y_i) v(x), \tag{8}$$

where $v(x)$ is an arbitrary function of the coordinate x, y_i is the transversal position of the impurity, and the magnitude of γ sets the magnitude of the impurity potential, which may be repulsive ($\gamma > 0$) or attractive ($\gamma < 0$). For the calculation of the wave function in the scattering region we will need to know the transverse energy levels $E_{n,s}$ (which define the bottoms of the subbands) in this region. These levels are obtained from

$$\sin(\alpha w) = \frac{\gamma}{\alpha} \sin(\alpha y_i) \sin[\alpha(y_i - w)] \tag{9}$$

as derived from the Schrödinger equation in the transverse direction, where $\alpha = (2mE)^{1/2}/\hbar$ and w is the width of the wire. For the impurity potential of Eq. (8) we can write the LSE Eq. (6) as

$$\psi_{\mathbf{p}}^{(+)}(x,y) = \psi_{\mathbf{p}}^{(0)}(x,y) + \gamma \int_{-\infty}^{\infty} dx' G^{(0)}(x,y;x',y_i) v(x') \psi_{\mathbf{p}}^{(+)}(x',y_i). \tag{10}$$

We note that the scattered wave function $\psi_{\mathbf{p}}^{(+)}(x,y)$ of Eq. (10) is expressed as the sum of the wave function for the incident wave $\psi_{\mathbf{p}}^{(0)}(x,y)$ plus a term that represents the effect of scattering. In order to be able to solve Eq. (10) and find the wave function $\psi_{\mathbf{p}}^{(+)}(x,y)$ throughout the entire wire we must know the wave function $\psi_{\mathbf{p}}^{(+)}(x',y_i)$ in the scattering region—i.e., in the region where $v(x') \neq 0$. Thus, our first goal is to find the wave function $\psi_{\mathbf{p}}^{(+)}(x',y_i)$ in the region where all the scattering takes place.

We assume that the scattering potential of Eq. (8) extends from $-x_0$ to x_0, that is $v(x') \neq 0$ for $|x'| \leqslant x_0$ and $v(x') = 0$ for $|x'| > x_0$. In the case where $v(x')$ has a Gaussian shape—i.e., $v(x') = e^{-x'^2/d^2}$, where d is the decay length of the scatterer—we can always choose $|x_0|$ far away such that $v(\pm x_0)$ becomes essentially zero. For the numerical calculations of the next section we choose $|x_0| = 5d$. For this value of $|x_0|$ it is clear that $v(\pm x_0)$ is very nearly zero. We divide the interval $[-x_0, x_0]$ into s equal subintervals of width $b = 2|x_0|/s$ and the coordinates x' and x of Eq. (10) are discretized according to $x' = -x_0 + qb$, $x = -x_0 + rb$, where $q, r = 0, 1, 2, \ldots, s$. The number s of subintervals can be chosen sufficiently large such that the results converge. In the case of a Gaussian impurity potential we found that convergence is obtained when the inequality $b < 0.1d$ is satisfied, which means that the number of intervals s should satisfy $s > 20|x_0|/d$. Replacing now the integral by a sum and setting $y = y_i$ in Eq. (10) we obtain

$$\psi_{\mathbf{p}}^{(+)}(-x_0 + rb, y_i) = \psi_{\mathbf{p}}^{(0)}(-x_0 + rb, y_i) + \gamma b \sum_{q=0}^{s} G^{(0)}(-x_0 + rb, y_i; -x_0 + qb, y_i) v(-x_0 + qb) \psi_{\mathbf{p}}^{(+)} \times (-x_0 + qb, y_i). \tag{11}$$

Equation (11) represents a set of s equations (one for each value of r) for the s unknown values of the wave function $\psi_{\mathbf{p}}^{(+)}$ and can be written (after some manipulations) in matrix notation as

$$\sum_{q=0}^{s} M_{rq} \psi_q^{(+)} = -\frac{1}{\gamma b} \psi_r^{(0)}, \tag{12}$$

where

$$M_{rq} = G^{(0)}(-x_0 + rb, y_i; -x_0 + qb, y_i) v(-x_0 + qb) - \frac{1}{\gamma b} \delta_{rq} \tag{13}$$

are the entries of an $s \times s$ matrix, which depend also on the electron energy [although this is not shown explicitly in Eq. (13)]. In Eq. (12) $\psi_q^{(+)}$ represents the unknown values of the wave function $\psi_{\mathbf{p}}^{(+)}(-x_0 + qb, y_i)$ in the scattering region and is a column vector. Similarly, $\psi_r^{(0)}$ is a column vector and represents the known values of the wave function $\psi_{\mathbf{p}}^{(0)}(-x_0 + rb, y_i)$ of the incident wave in the region of the scattering potential. Inverting the matrix $[\mathbf{M}]$ whose elements are given in Eq. (13) allows us to solve Eq. (12) for $\psi_q^{(+)}$ and find the wave function in the scattering region (which was our primary goal). This solution is written formally as

$$[\psi_q^{(+)}] = -\frac{1}{\gamma b} [\mathbf{M}]^{-1} [\psi_r^{(0)}]. \tag{14}$$

Having found the values of the wave function $\psi_{\mathbf{p}}^{(+)}(x, y_i)$ that we needed we can proceed and perform the integral in Eq. (10) by discretization (in line with the above discussion) and thus determine the wave function to the right (or left) of the scattering potential (that is, for $|x| > x_0$). The wave function transmission amplitudes are then extracted from that part of the wave function valid for $x > x_0$ and given formally as

$$t_{nn'}(E) = \delta_{nn'} + \frac{\gamma b}{2ik_{n'}} \sqrt{2\pi} \phi_{n'}(y_i) \sum_{q=0}^{s} e^{-ik_{n'}(-x_0 + qb)} v(-x_0 + qb) \psi_{\mathbf{p}}^{(+)}(-x_0 + qb, y_i), \tag{15}$$

where n and n' are the incident and scattered modes respectively, and $\psi_{\mathbf{p}}^{(+)}(-x_0 + qb, y_i)$ are the values of the wave function in the scattering region found from Eq. (14). By setting $k_{n'} = i\kappa_{n'}$ in Eq. (15) we obtain the wave function amplitude for the case in which mode n' is an evanescent mode. The current transmission coefficients $T_{nn'}$ through the impurity are obtained as

$$T_{nn'} = \frac{k_{n'}}{k_n} t_{nn'} t^*_{nn'}. \tag{16}$$

Equation (16) gives the probability that an electron incident from mode n on the left will emerge in mode n' on the right. In order to calculate the conductance we use Landauer's formula:[30,31]

$$G = \frac{2e^2}{h} \sum_{n,n'} T_{nn'}, \tag{17}$$

where n and n' run only over the propagating modes of the wire.

III. CONDUCTANCE OF A QUANTUM WIRE WITH A GAUSSIAN IMPURITY

In this section we present results for the effects of a Gaussian impurity potential on the conductance of a 2D rectilinear quantum wire. In particular for the impurity potential we will employ the model

$$V_i(x,y) = \frac{\hbar^2 \gamma}{2m^*} \delta(y - y_i) e^{-x^2/d^2}, \tag{18}$$

which is extremely localized along the y direction but has a decay length d along the propagation direction. The laterally confining potential of the wire is that of an infinite square well. The cross section (width w) is uniform along the wire. The electron mass is taken to be the effective mass for GaAs which is 0.067 of the free-electron mass. In the following numerical calculations we include a total of eight modes. Including higher modes does not affect the results especially as the size of the impurity increases. In the clean part of the wire (i.e., outside the scattering region) the infinite square well confining potential $V_c(y)$ gives rise to the transverse energy levels $E_n = \hbar^2 \pi^2 n^2 / 2m^* w^2$. We will express all distances in units of the wire width w and all energies will be measured in units of E_1.

A. Conductance through a repulsive Gaussian impurity

We analyze now the influence of the Gaussian impurity potential on the conductance. The transverse location of the impurity is at $y_i = (5/12)w$. As mentioned in Sec. II the choice $|x_0| = 5d$ is sufficient to guarantee that $V_i(\pm x_0, y) = 0$. The energy subbands in the scattering region (which we will denote as $E_{n,s}$) are shifted upwards due to the transverse potential of the impurity. The first subband in this region opens at $E_{1,s} = 1.85E_1$ while the second opens at $E_{2,s} = 4.35E_1$.

Figure 1(a) shows the behavior of the conductance through a Gaussian impurity in the 2D rectilinear quantum wire plotted versus the Fermi energy over the first subband, for several different values of the parameter d/w. For the smallest value of d chosen in the calculation (i.e., $d = 0.3w$ which corresponds to the solid line) we see that G increases almost linearly in the beginning and finally approaches the quantum unit $2e^2/h$. However increasing the value of d leads to a progressively sharper rise of the conductance at the opening of the subband $E_{1,s}$ and a corresponding suppression of the conductance below $E_{1,s}$. For $E_1 < E < E_{1,s}$ the first channel is not propagating and therefore transport occurs via tunneling for this particular channel. While the first channel of propagation opens up at $E_{1,s}$, the subbands above the Fermi level contribute to some extent by tunneling. Thus at a particular value of d the effect of the evanescent states above the Fermi level is to give rise to electron transmission prior to the opening of the subband $E_{1,s}$. The suppression of the conductance (for $E_1 < E < E_{1,s}$) with increasing d can be understood simply in terms of the progressively smaller contribution of evanescent modes. We illustrate this gradual decrease of tunneling in Fig. 1(b) for two values of the energy $E = 0.9E_{1,s}$ and $0.88E_{1,s}$, i.e., well below the bottom of the first subband $E_{1,s}$. As it is clear from Fig. 1(b) the tunneling probability (which is smaller for lower energies) decreases exponentially and for large enough values of d it will vanish. Immediately after the opening of the subband $E_{1,s}$ and with increasing values of d the conductance approaches progressively faster the quantum unit $2e^2/h$ and equals $2e^2/h$ over a larger part of the subband. This is due to the suppression of backscattering as the impurity potential becomes smoother. Thus the simultaneous suppression of tunneling and backscattering effects with increasing d results in a sharper conductance step. In the extreme case in which d becomes very large (i.e., the impurity potential becomes almost flat) it is reasonable to expect that the impurity will cause very little or

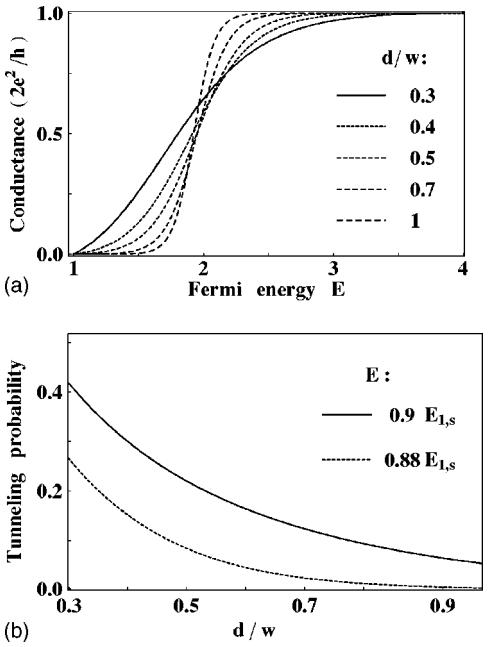

FIG. 1. (a) Conductance G (in units of $2e^2/h$) as a function of Fermi energy E (over the first subband) through a Gaussian impurity of strength $\gamma = 2.5 \times 10^6$ cm^{-1} in a 2D rectilinear quantum wire of width w. E is given in units of E_1 (where E_1 is the bottom of the first subband in the clean wire). Results are shown for various sizes of the impurity (specified by the parameter d/w). Note that increasing d results to sharper rise of the conductance. (b) Tunneling probability vs d/w, for two values of the Fermi energy. The solid line corresponds to $E = 0.9E_{1,s}$ while the dashed line to $E = 0.88E_{1,s}$, where $E_{1,s}$ is the bottom of the first subband in the scattering region.

no reflection since the quantum wavelength becomes small compared with the characteristic distance over which the potential varies appreciably. In this case quantum tunneling will also be absent resulting to zero transmission prior to the opening of $E_{1,s}$. Accordingly we will obtain perfectly sharp step structure and $G=2e^2/h$ over the entire subband. In the opposite limit of very small d the conductance of a point scatterer is recovered. It is worth mentioning here that in the case of a point scatterer there is only one set of subbands in the wire and the first two channels become propagating exactly at $E=E_1$ and $E=E_2$, respectively.

The above points can also be discussed in a perturbation picture. In particular, the reflection coefficients due to the backscattering can easily be calculated in the first-order Born approximation,[22] obtaining

$$R_{nn'}(E) = \frac{\Gamma_{nn'}^2 \pi d^2}{4k_n k_{n'}} e^{-(k_n + k_{n'})^2 d^2/2}, \tag{19}$$

where n and n' are the incident and reflected modes, respectively, while $\Gamma_{nn'} = \gamma \phi_n(y_i) \phi_{n'}^*(y_i)$ are constants that are proportional to the coupling of the incident and reflected transverse modes at the impurity. It is clear from Eq. (19) that backscattering reduces very fast with increasing d, leading to gradual enhancement of transmission and improving the quantized conductance step. In fact in the limit in which d becomes very large [while keeping all other parameters in Eq. (19) fixed], $R_{nn'}$ approaches zero, as can be verified from the above equation. For later analysis we also note that the above reflection coefficients also depend on the coupling of the transverse modes at the impurity position through the constants $\Gamma_{nn'}$.

As mentioned above the subbands that lie above the Fermi level can contribute to the conductance by tunneling. The most important contribution comes from the first subband that lies immediately above the Fermi level (since the contribution of the higher ones decreases with increasing energy). However, this contribution is different for different conductance steps. This effect is illustrated in Fig. 2 where we plot the conductance versus the Fermi energy over the first two subbands, for several different values of the decay length d. It is seen that the first conductance step rises smoother in the vicinity of $E_{1,s}$ than the corresponding rise of the second step in the vicinity of $E_{2,s}$. This can be understood if we examine the distance between the subbands in the scattering region and those in the clean wire. The distance $\Delta E^{(1)}$ between E_1 and $E_{1,s}$ is $0.85E_1$, which is much larger than the distance $\Delta E^{(2)}$ between E_2 and $E_{2,s}$, which is $0.35E_1$. Even though the larger distance $\Delta E^{(1)}$ leads to smaller tunneling probability for $E_1 < E < E_{1,s}$, the tunneling region $\Delta E^{(1)}$ of the first step is much greater than the tunneling region $\Delta E^{(2)}$ of the second step by a factor of 2.42. Thus in the second step there is a larger amount of tunneling in a smaller tunneling region and this leads to rapid enhancement of the conductance values in this region.

The smoother and sharper rise of the first and second steps, respectively, is also due to the different strength of the interaction of the respective modes with the impurity. For the particular position of the impurity that we consider [i.e., $y_i = (5/12)w$] the coupling of the first mode at the impurity is stronger than the corresponding coupling of the second mode. Consequently scattering of the first mode is enhanced while scattering of the second mode is suppressed, giving rise to smoother and sharper steps, respectively. This can also be understood from the perturbation result of Eq. (19). We must note that when we consider transport in the second subband there is intrasubband reflection through R_{12}, R_{21} in addition to R_{11}. However, the dominant contribution comes from the backscattering within the second channel, i.e., from R_{22}, which has the smallest wave vector as can be seen from Eq. (19). Now when we consider transport in the first subband the magnitude of Γ_{11} is large resulting to enhanced reflection. When we consider transport in the second subband the coupling constant Γ_{22} (corresponding to the dominant reflection coefficient R_{22}) is small leading to reduced reflection. Placing the impurity on the central axis of the wire would result in a maximum scattering of the first mode while the second will suffer no scattering, leading to almost perfect quantization of the second step. These points will become more clear in the next section where we examine the influence of the impurity position on the conductance.

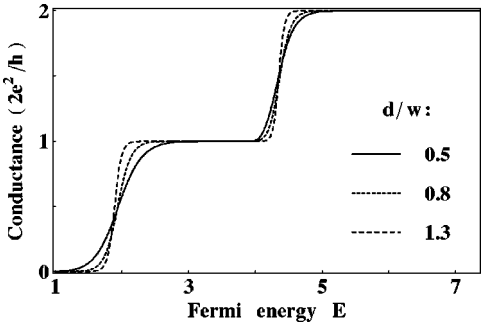

FIG. 2. Conductance G (in units of $2e^2/h$) vs Fermi energy E through a Gaussian impurity of strength $\gamma=2.5\times10^6$ cm^{-1} in a 2D rectilinear quantum wire of width w, for three values of the parameter d/w. Note the sharper rise of the second conductance step (compared to the first step) which is due to the smaller distance between $E_{2,s}$ and E_2, where $E_{2,s}$ is the bottom of the second subband in the scattering region and E_2 is the corresponding subband in the clean part of the wire.

B. Effects of the impurity position on the conductance

Several interesting effects are observed when we vary the transverse position of the impurity. In Fig. 3(a) we show the conductance through a Gaussian impurity with $d=0.7w$ in a 2D rectilinear quantum wire plotted versus the Fermi energy, for three different impurity positions y_i. It can be seen that as the impurity is displaced away from the central axis of the wire the position of the first conductance step is systematically shifted towards lower energy values while it rises progressively sharper at the opening of the subband $E_{1,s}$. Note in particular that when the impurity is placed at $y_i=(1/12)w$ the conductance grows rapidly with energy and very soon approaches values very close to the quantum unit $2e^2/h$. However, the shifting of the position of the second conductance step can be either towards lower or higher energy values

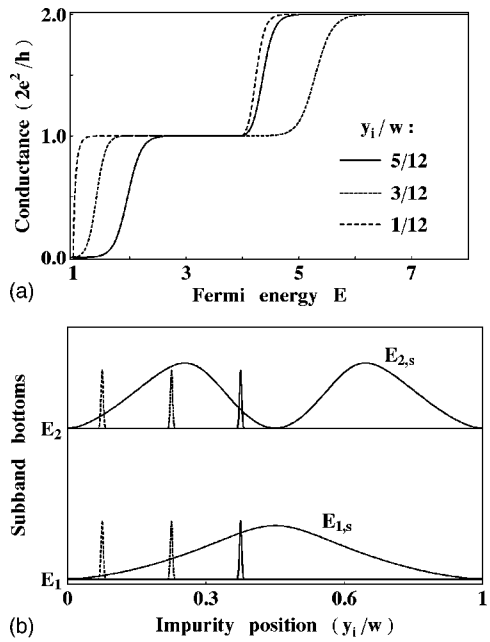

FIG. 3. (a) Conductance G (in units of $2e^2/h$) vs Fermi energy E through a Gaussian impurity of strength $\gamma=2.5\times10^6$ cm^{-1} and $d=0.7w$ in a 2D quantum wire of width w, for three different impurity positions (specified by the parameter y_i/w). Note the shifting of the positions of the conductance steps which is due to the shifting of the subbands $E_{n,s}$ in the scattering region. (b) The bottoms of the first two subbands vs impurity position y_i/w. The two straight horizontal lines represent the subbands E_1, E_2 of the clean wire while $E_{1,s}$, $E_{2,s}$ are the subbands in the scattering region which follow the structure of the transverse wave functions $|\phi_n(y)|^2$.

(depending on y_i) while the rise of this step may be smoother or sharper.

These effects can be understood simply by examining the behavior of the (transverse) energy levels $E_{1,s}$ and $E_{2,s}$ as a function of the impurity position which is illustrated in Fig. 3(b). While E_1 and E_2 (shown by the straight horizontal lines) assume constant values (independent of y_i), $E_{1,s}$ and $E_{2,s}$ are functions of the impurity position. In fact the energy levels $E_{n,s}$ versus the impurity position y_i follow the structure of the squared modulus of the transverse wave functions (i.e., the structure of $|\phi_n(y)|^2$). The physical origin for the shifting of the bottoms of the subbands $E_{n,s}$ can be understood simply in a perturbation picture where the first order correction $(\hbar^2\gamma/2m)|\phi_n(y_i)|^2$ to the unperturbed levels E_n is proportional to the interaction of the transverse wave functions at the impurity position. The structure of the subband $E_{1,s}$ is identical to the squared modulus of the first mode $\phi_1(y)$ while that of the second subband $E_{2,s}$ is identical to the squared modulus of the second mode $\phi_2(y)$. Higher subbands also exhibit analogous behavior. Now as the impurity is moved from $0.5w$ to 0 the first subband $E_{1,s}$ gradually shifts towards lower energies [see Fig. 3(b)], leading to a corresponding shifting of the position of the first conductance step observed in Fig. 3(a). However, the second subband $E_{2,s}$ first increases, reaches its maximum value at $y_i=0.25w$, and then decreases until $E_{2,s}=E_2$ at $y_i=0$. Consequently displacing the impurity from $0.5w$ to 0 leads first to an upward (until $0.25w$) and then to a downward shifting of the position of the second quantum step, as it is in fact observed in Fig. 3(a). Thus the greater the coupling of a particular transverse mode at the impurity the greater the shifting of the corresponding subband. Note also that for an impurity on the central axis of the wire $E_{2,s}=E_2$.

The sharper or smoother rise of the conductance steps for different impurity positions observed in Fig. 3(a) can be explained in terms of the structure of the subbands. The three impurity positions $y_i=(5/12)w$, $(3/12)w$, and $(1/12)w$ for which we calculated the conductance are shown in Fig. 3(b) as three spikes in their respective positions. The gradually sharper rise of the first conductance step (as the impurity is displaced away from the central axis of the wire) is partly due to the progressively shorter tunneling region (since the distance between $E_{1,s}$ and E_1 continuously decreases) and also due to the progressively weaker coupling of the transverse wave function at the impurity position. When the impurity is located at $(5/12)w$ (i.e., close to the central axis of the wire) the interaction of the first mode with the impurity is strongest leading to enhanced scattering effects and smooth first conductance step. However, when the impurity is placed at $(1/12)w$ the interaction of the first mode with the impurity becomes much weaker [as can be seen from Fig. 3(b)], leading to suppression of scattering effects and sharper conductance step.

Similarly by examining the structure of $E_{2,s}$ we can explain the characteristics of the second conductance steps. When the impurity is placed at $(3/12)w$ it is seen in Fig. 3(a) that the slope of the rise of the second quantum step becomes smaller which is partly due to the wider tunneling region [i.e., the distance between $E_{2,s}$ and E_2 becomes large, as shown in Fig. 3(b)] and also due to the stronger interaction of the second mode with the impurity. It is also worth mentioning that the impurity positions $(5/12)w$ and $(1/12)w$ are entirely equivalent as far as the second mode is concerned. This means that for those two impurity positions the opening of the second subband occurs at exactly the same energy and the coupling Γ_{22} of the second mode at the impurity is also exactly the same. However, for $y_i=(1/12)w$ the second step is slightly sharper. This is due to the fact that while we consider transport at the second subband the first mode still contributes to the conductance and the coupling of this mode with the impurity is weaker for $y_i=(1/12)w$ [see Fig. 3(b)], resulting in reduced scattering and slightly enhanced transmission.

To this end, we emphasize that the effects of the impurity position just discussed are particularly important in the detailed structure of the conductance and they have also been examined in various other systems with different types of impurities.[8,16,22,32] Comparing the above results with the results for a point scatterer in the wire we note some differences. First, the Gaussian impurity model employed in this paper causes a delay in the opening of a new channel which is due to the presence of a second set of subbands $E_{n,s}$ in the scattering region. In contrast, when a point impurity is present in the quantum wire the opening of a channel occurs precisely at the subband bottoms E_n of the unperturbed wire. Second, the transverse position of the Gaussian impurity has

a greater influence on the conductance of the wire because of the possible shifting of the subbands (in the scattering region) as the impurity is displaced. For some impurity positions the subbands in the scattering region are far apart from those of the unperturbed wire while for other positions they coincide resulting in significant changes in the appearance of the conductance. This effect is absent from the point impurity model where only one set of subbands exists. We next turn to the case where the impurity is attractive.

C. Attractive Gaussian impurity

We examine now the influence of an attractive Gaussian impurity on the conductance of a 2D rectilinear quantum wire. We show that in this case there exist multiple dips in the conductance that are due to the formation of quasibound (resonant) states in the continuum and their interaction with the continuum states. In the subsequent analysis we confine our attention to the behavior of these dips as a function of the decay length of the impurity. The first subband in the scattering region opens at $E_{1,s}=-0.51E_1$, the second at $E_{2,s}=3.15E_1$, and the third at $E_{3,s}=6.92E_1$.

In Fig. 4(a) we show the conductance plotted versus the Fermi energy, for three different values of the decay length d and the upper two curves (corresponding to $d/w=0.48$ and 0.56) are vertically offset by an amount $1.1(2e^2/h)$ and $2.2(2e^2/h)$, respectively, for clarity. We note that as d increases multiple resonance dips appear in the first and the second subbands. The number of these dips increases with increasing d. As mentioned above the dips in the conductance are explained in terms of the formation of quasibound states—at special energies—in the impurity region. Electrons at those energies spend enhanced periods of time in the impurity region (i.e., they become temporarily trapped in the quasibound states), and destructive interference of these states with the continuum states causes the conductance to drop resulting in a complete interference blockade of the electron transport at E_{res}.

Two important quantities related to resonant scattering are E_{res} and the sharpness of the resonance which is quantified by the half width Γ. In fact, since the resonances are only possible at positive collision energies E_{res}, the corresponding quasibound state energies E_{qb} are situated below the positive real axis of the complex E plane:

$$E_{qb} = E_{res} - i\frac{\Gamma}{2}. \tag{20}$$

The half width Γ determines the lifetime τ of the quasibound state through the relation $\tau=\hbar/\Gamma$. In Fig. 4(b) we show the location of the first dip E_{res} in the first subband plotted versus the decay length d. The corresponding evolution of the half width (denoted by HW) of this resonant dip versus d is shown in Fig. 4(c). We note that increasing the value of d causes shifting of the dip location E_{res} toward lower energies while the half width shows a decaying oscillatory behavior. The decrease of E_{res} is due to the increasingly larger integrated strength of the impurity $\sim\gamma d$, which results in a progressively larger perturbation to the unperturbed electron transport and thus to a larger binding energy (which is the energy difference between the quasibound state and the first subband from which it is split off). A similar effect occurs in the case of an attractive δ-function impurity in a quantum wire,[23] where the dip can move lower in energy when the strength of the impurity increases. This last observation implies that E_{res} in the conductance through a Gaussian impurity can decrease when either the strength γ or the decay length d increases. The occurrence of the dips is also closely related to the position of the impurity. We verified that placing the impurity on the central axis of the wire causes the disappearance of the dips in the first subband. This is similar to the case of a δ-function scatterer,[6,22–24] where the binding energy besides being proportional to the strength of the impurity is also proportional to the coupling of the next higher mode at the impurity position. In analogy with the δ-function

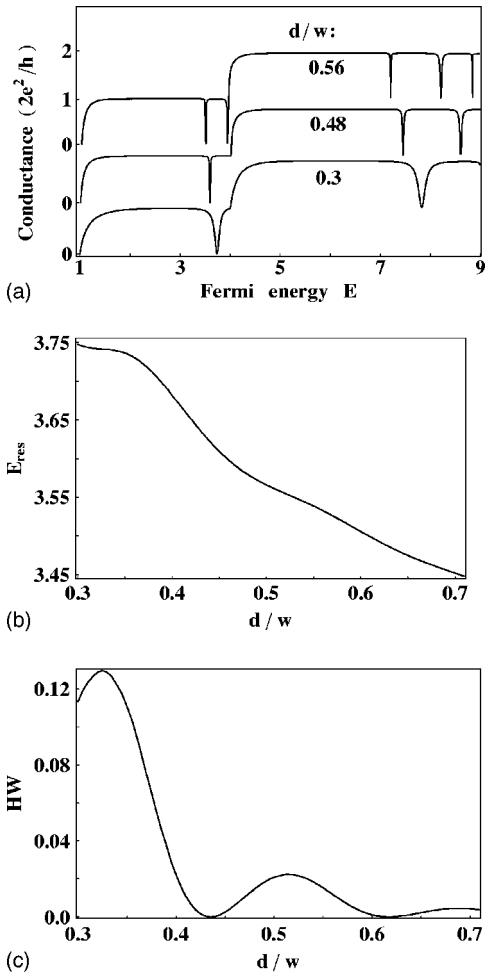

FIG. 4. (a) Conductance G (in units of $2e^2/h$) vs Fermi energy E through an attractive Gaussian impurity of strength $\gamma=-2\times10^6$ cm^{-1} in a 2D quantum wire of width w, for three values of the parameter d/w. The multiple dips in the conductance are due to the formation of quasibound states. The upper two curves (corresponding to $d/w=0.48$ and 0.56) are vertically offset by an amount $1.1(2e^2/h)$ and $2.2(2e^2/h)$ respectively. (b) Location of the first dip E_{res} (in units of E_1) in the first subband vs the size of the impurity (specified by the parameter d/w). (c) Half width Γ (in units of E_1) vs d/w. The two minima in the HW correspond to highly localized states with enhanced lifetime.

scatterer we argue that the disappearance of the dips (when the impurity is on the axis) is caused by the vanishing coupling of the second mode at the impurity.

In Fig. 4(c) it is seen that the half width as a function of d first increases, reaches a maximum at $d=0.325w$ (where $\Gamma_{max}=0.1246E_1$), and then decreases to a minimum at $d=0.4352w$ (where $\Gamma_{min}\approx 2\times 10^{-6}E_1$) after which it grows again. This situation can be repeated a few times (depending on the properties of the impurity, such as its strength as well as its transverse position). The extremely narrow half width of the resonant dip at $d=0.4352w$ corresponds to a very stable state—a state with greatly enhanced lifetime. Physically this highly localized state is stable since at the particular value of d its interaction with the continuum is minimized and therefore it decays extremely slowly (i.e., the decay rate of the localized state into a propagating state is lowest). Thus at this special value of d transformation of the quasibound state to a highly localized state occurs. The dips in the second subband also exhibit similar behavior.

The increase of the degree of localization of the quasibound states as $\Gamma\rightarrow 0$ can be explained in terms of the coherent interaction of interfering channels in the impurity region. This can be understood if we consider the energy interval $E_{2,s}<E<E_2$ where there are two propagating modes $n=1,2$ in the impurity region, while outside this region and for the same energy interval only mode $n=1$ is propagating while mode $n=2$ turns into an evanescent wave. Accordingly the coherent resonant interaction of these channels leads to an increase of the charge density in the region of localization and the electron escape rate is minimum.

Long-living electron states were also predicted for a rectangular well model for the impurity potential in a straight quantum waveguide,[19] and the subsequent collapse of the Fano resonance was studied in detail. The coherent resonant phenomena in the impurity region is also the physical origin of the effects studied in Ref. 19.

It is also useful to discuss the dips of the conductance in terms of the squared modulus of the wave function $|\psi_{\mathbf{p}}^{(+)}\times(x,y)|^2$. In Fig. 5 we show $|\psi_{\mathbf{p}}^{(+)}(x,y)|^2$ as a function of x and y. Figure 5(a) corresponds to the conductance minimum in the first subband of the lower curve in Fig. 4(a), which occurs at $E_{res}=3.7363E_1$, while Fig. 5(b) corresponds to the conductance minimum in the first subband of the middle curve in Fig. 4(a), which occurs at $E_{res}=3.5805E_1$. The Gaussian impurity extends from $-x_0$ to x_0. In Fig. 5(a) we note that the waves inside the impurity region decay towards the back end of the impurity and for $x<-x_0$ the incident waves interfere with the reflected waves to produce the pattern observed. However, in Fig. 5(b) $|\psi_{\mathbf{p}}^{(+)}(x,y)|^2$ inside the scattering region has much larger magnitude compared to the amplitude of the interfering waves for $x<-x_0$, and this state is more stable, leading to a smaller half width of the corresponding resonant dip. Figure 5(c) corresponds to the minimum of the conductance at the critical value of $d=0.4352w$ with energy $E_{res}=3.6263E_1$ for which the half width approaches zero. We must note that for $x<-x_0$ in Fig. 5(c) there are also reflected waves which interfere with the incident waves. However, this interference pattern is not discernible due to the greatly enhanced magnitude of $|\psi_{\mathbf{p}}^{(+)}(x,y)|^2$ in the impurity region. The extremely small interaction of this very stable state with the propagating states leads to a very small escape probability and hence to an infinitesimal resonance width.

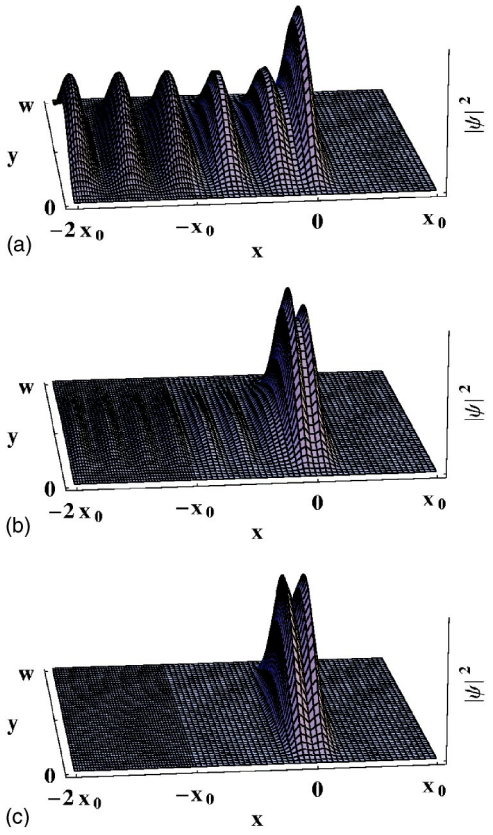

FIG. 5. Three-dimensional plots of the squared modulus of the wave function $|\psi_{\mathbf{p}}^{(+)}(x,y)|^2$ vs x and y. (a) corresponds to the conductance minimum in the subband of the lower curve in Fig. 4(a) which occurs at $E_{res}=3.7363E_1$ while (b) corresponds to the minimum in the first subband of the middle curve in Fig. 4(a) and occurs at $E_{res}=3.5805E_1$. (c) corresponds to the stable state with infinitesimally small half width [i.e., the first minimum in Fig. 4(c)] which corresponds to $d=0.4352w$ and $E_{res}=3.6263E_1$.

The formation of the long-living electron states discussed above should be observable in high-mobility channels as for example in a narrow channel made of $GaAs/Al_xGa_{1-x}As$ heterostructures. A finite-size impurity may artificially be created in the quantum wire using nanotechnology.[33]

We would like to further discuss the results shown in Fig. 4(a). It is well known that the presence of an attractive impurity in a quantum wire structure leads to the creation of quasibound levels in the continuum, which in turn give rise to resonance line shapes in the conductance versus Fermi energy.[34] The most general resonant line shape that appears in these systems is described by the asymmetric Fano function[35]

$$f(\epsilon)=\frac{1}{1+q^2}\frac{(\epsilon+q)^2}{\epsilon^2+1}, \tag{21}$$

where $\epsilon=(E-E_R)/\Gamma$ is the energy from resonance, Γ is the resonance width and q is the asymmetry parameter. In quasi-

one-dimensional systems it has been shown[36] that the transmission coefficient can be expressed in the Fano form as given in Eq. (21), and in this case the asymmetry parameter $q=(E_R-E_0)/\Gamma$, where E_R is the resonance energy and E_0 is the energy of the transmission zero. As mentioned in the beginning of this section the dips in the conductance curves of Fig. 4(a) are due to the formation of quasibound states in the continuum and their subsequent coupling with the continuum states. However, instead of the occurrence of asymmetric Fano resonances we observe symmetric dips. This behavior of the conductance indicates that the asymmetry parameter q must be negligible (i.e., $q \ll 1$), which means that the distance between the energy of the transmission zero E_0 and the resonance energy E_R is infinitesimal. Equivalently we may say that the symmetric dips in Fig. 4(a) are due to the large background[36] (i.e., nonresonant) transmission, which leads to infinitesimal values of q. For the attractive Gaussian impurity that we considered in this section we verified numerically that the background transmission rises progressively faster as the decay length d increases (i.e., as the impurity potential becomes smoother) and for sufficiently large d it becomes unity over the largest part of the energy subband, thereby leading to symmetric dips in the conductance curves. We fully illustrate these considerations in the next section where we employ the Feshbach[37] approach (which is particularly suitable for the description of resonance line shapes) in order to calculate the transmission coefficient and the asymmetry parameter in the case of a second-type impurity potential which is very similar (almost identical) to the Gaussian but having also a lateral extension. It will also be shown that in the regime of relatively small values of the decay length an asymmetric Fano resonance appears in the transmission.

D. Two-channel Feshbach approach

In this section we employ the Feshbach approach in order to describe the transmission resonances in a rectilinear quantum wire with a smooth finite-size impurity to be defined below. Feshbach's theory of coupled scattering channels was in fact reformulated and employed in quasi-one-dimensional systems in order to describe symmetric[34] line shapes (Breit-Wigner-type resonances) and also to describe more general asymmetric[36] line shapes for arbitrary coupling potentials, providing microscopic expressions for all line shape parameters.

As in Sec. II we consider a uniform quantum wire where the electrons are confined along the y direction but are free to propagate along the x direction. In the presence of an impurity we need to solve the Schrödinger equation

$$\left[-\frac{\hbar^2}{2m^*}\nabla^2 + V_c(y) + V_i(x,y)\right]\Psi(x,y) = E\Psi(x,y), \quad (22)$$

where $V_c(y)$ is the confining potential and $V_i(x,y)$ is the attractive impurity potential, which we take to be of the form

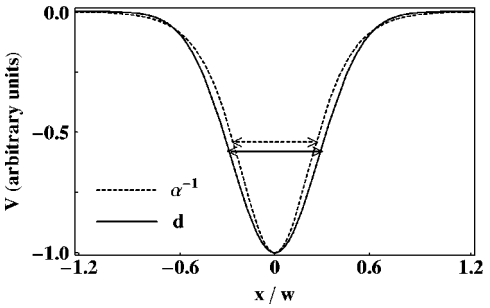

FIG. 6. Impurity potential profiles versus x/w. The solid line represents the Gaussian impurity potential with decay length d while the dashed line represents the impurity potential $V(x)=\mathrm{sech}^2(\alpha x)$ with decay length $\alpha^{-1}=3^{1/3}d/\sqrt{\pi}$ (as explained in the text).

$$V_i(x,y) = \frac{\hbar^2\gamma}{2m^*}\mathrm{sech}^2(\alpha x)\upsilon(y), \quad (23)$$

where $v(y)$ is an arbitrary function of the coordinate y, α^{-1} is the decay length, and $\gamma<0$. The longitudinal part of the impurity potential given in Eq. (23) has smooth profile and is very similar to the Gaussian potential as shown in Fig. 6 [where the solid line represents the Gaussian function while the dashed line is the function $\mathrm{sech}^2(\alpha x)$]. In fact we can make the two potentials almost identical by forcing the square roots of the variances Δx of the two potentials to be equal to each other. For a given value of the decay length d of the Gaussian potential the above condition leads to $\alpha^{-1}=3^{1/3}d/\sqrt{\pi}$. The confining potential $V_c(y)$ along the y direction (which is taken to be an infinite square well) gives rise to modes $\phi_n(y)$. We expand the wave function $\Psi(x,y)$ of Eq. (22) in terms of the modes $\phi_n(y)$:

$$\Psi(x,y) = \sum_{n=1}^{\infty} \psi_n(x)\phi_n(y). \quad (24)$$

Substitution of Eq. (24) into Eq. (22) in the usual way leads to the coupled-channel equations for $\psi_n(x)$,

$$(E - E_n - \hat{K})\psi_n(x) = \sum_{l=1}^{\infty} V_{nl}(x)\psi_l(x), \quad (25)$$

where $\hat{K}=-(\hbar^2/2m^*)d^2/dx^2$ and the coupling matrix elements $V_{nl}(x)$ are given as

$$V_{nl}(x) = \int dy\,\phi_n(y)V_i(x,y)\phi_l(y). \quad (26)$$

For the particular impurity potential given in Eq. (23) these matrix elements take the form

$$V_{nl}(x) = \frac{\hbar^2\gamma}{2m^*}\mathrm{sech}^2(\alpha x)\upsilon_{nl}, \quad (27)$$

where $\upsilon_{nl}=\langle\phi_n|\upsilon(y)|\phi_l\rangle$. Far away from the impurity we have $V_{nl}(\pm\infty)=0$.

We consider the case $E_1 \leqslant E \leqslant E_2$ for which only the first channel can propagate along the wire while the second can

contribute via tunneling. Thus only the first channel $n=1$ can be in some scattering state. These scattering states are given as solutions of the equation

$$(\hat{K}+V_{11})\chi_k^{\pm}(x)=(E-E_1)\chi_k^{\pm}(x), \tag{28}$$

where χ_k^+ and χ_k^- correspond to scattering states for which the incident wave comes from $-\infty$ and $+\infty$, respectively. These states describe the background (nonresonant) scattering, which is the scattering in a hypothetical system where the coupling to the bound state is absent.[12,36] The solution to Eq. (28) proceeds in the same way as in a one-dimensional scattering problem[38] with an attractive potential $-U_{11}\,\mathrm{sech}^2(\alpha x)$, where $U_{11}=-(\hbar^2\gamma/2m^*)v_{11}$, and the asymptotic form of the wave function as $x\to-\infty$ is given in terms of Gamma functions

$$\chi_k^+(x)\sim e^{-ikx}\frac{\Gamma(ik/\alpha)\Gamma(1-ik/\alpha)}{\Gamma(-s)\Gamma(1+s)} + e^{ikx}\frac{\Gamma(-ik/\alpha)\Gamma(1-ik/\alpha)}{\Gamma(-ik/\alpha-s)\Gamma(-ik/\alpha+s+1)}, \tag{29}$$

where $k=[2m^*(E-E_1)]^{1/2}/\hbar$ and $s=(1/2)[-1+\sqrt{1+(8m^*U_{11}/\alpha^2\hbar^2)}]$. Then the scattering states can be written in the form

$$\chi_k^{\pm}(x)=\begin{cases} t^{bg}e^{\pm ikx} & (x\to\pm\infty) \\ e^{\pm ikx}+r_{\pm}^{bg}e^{\mp ikx} & (x\to\mp\infty) \end{cases}, \tag{30}$$

where the upper signs correspond to incident wave from $-\infty$. t^{bg} and $r_{\pm}^{bg}$ correspond to the background transmission and reflection amplitudes in the wire. Specifically, r_+^{bg} is the ratio of coefficients in the function $\chi_k^+(x)$ of Eq. (29). Due to symmetry $r_-^{bg}=r_+^{bg}$ holds. We consider E close to E_0, where E_0 is the bound state energy of the state Φ_0 in the potential $V_{22}(x)$ of the uncoupled channel $n=2$, i.e.,

$$(\hat{K}+V_{22})\Phi_0(x)=(E_0-E_2)\Phi_0(x). \tag{31}$$

Employing the notation $\epsilon=[-2m^*(E_0-E_2)]^{1/2}/\hbar\alpha$, $s=(1/2)\times[-1+\sqrt{1+(8m^*U_{22}/\alpha^2\hbar^2)}]$, and $U_{22}=-(\hbar^2\gamma/2m^*)v_{22}$, Eq. (31) can be brought to a form[38] that has solutions the associated Legendre polynomials $P_s^{\epsilon}(\xi)$, where $\xi=\tanh(\alpha x)$. The energy levels are then determined by the condition $\epsilon=s-p$, which gives

$$E_p=E_2-\frac{\hbar^2\alpha^2}{8m^*}\left[-(1+2p)+\sqrt{1+\frac{8m^*U_{22}}{\alpha^2\hbar^2}}\right]^2, \tag{32}$$

where $p=0,1,2,\ldots$ There is a finite number of levels determined by the condition $\epsilon>0$, i.e., $p<s$. In the following we assume that U_{22} and α are such that $s\leqslant 1$, which implies that there is only one bound state with energy E_0. The normalized bound state wave function that corresponds to this energy level is $\Phi_0(x)=(\alpha/2)^{1/2}\mathrm{sech}(\alpha x)$.

At this point it becomes clear that the reason we employed the impurity potential of Eq. (23) in this section is that it allows us to find analytical solutions to Eqs. (28) and (31) for the scattering and bound states whereas this would not be possible for the Gaussian potential (for which no analytical solution exists in one dimension). This will allow us to study in detail the characteristics of the resonance line shape in the two-channel approximation. On the other hand, the LSE could also have been used to solve numerically the problem for a Gaussian impurity with an arbitrary but specific shape of the impurity in the transverse direction. However this would not permit us to vary the intra- and intersubband coupling matrix elements independently [as we will be able to do for the impurity of Eq. (23) for which $v(y)$ is completely arbitrary], which are in fact buried inside the scattering wave function of Eq. (14).

We now make the approximation of truncating the sum in Eq. (25) at $n=2$. We then get the system of equations

$$(E-E_1-\hat{K}-V_{11})\psi_1(x)=V_{12}\psi_2(x), \tag{33}$$

$$(E-E_2-\hat{K}-V_{22})\psi_2(x)=V_{21}\psi_1(x). \tag{34}$$

The coupled-channel equations (33) and (34) are solved in general in Refs. 34 and 36 with the ansatz $\psi_2(x)=A\Phi_0(x)$ and employing the retarded Green's operator for Eq. (33). In the Appendix we calculate the wave function $\psi_1(x)$ in the quantum wire for $x\to\infty$ with the impurity potential of Eq. (23) and extract the transmission coefficient

$$T=|t^{bg}|^2\frac{(E-E_0)^2}{(E-E_0-\delta)^2+\Gamma^2}, \tag{35}$$

where δ and Γ are given in Eqs. (A12) and (A13) of the Appendix. Equation (35) is of the Fano form in which the real quantity δ determines the asymmetry parameter q of the line shape by the relation

$$q=\frac{E_R-E_0}{\Gamma}=\frac{\delta}{\Gamma}=-\frac{\cos[(\pi/2)\sqrt{1+(8m^*U_{11}/\hbar^2\alpha^2)}]}{\sinh(\pi k/\alpha)}. \tag{36}$$

An important feature of Eq. (36) is that $q\to 0$ as the decay length α^{-1} increases (since the denominator grows progressively faster while the numerator is restricted between the values of -1 and 1). This effect is more pronounced when the wave vector k is larger (i.e., when the asymmetric resonance line shape occurs closer to the second subband threshold). A second important feature of Eq. (36) is that for suitable values of U_{11}/α^2 the quantity δ can be positive, negative or zero (i.e., the resonance energy may occur before, after or be equal to the energy of the transmission zero). It can be shown that for $U_{11}/\alpha^2=(\hbar^2/8m^*)[(2n+1)^2-1]$ where $n=1,2,\ldots$, we have $E_R=E_0$ and in this case the transmission exhibits symmetric Breit-Wigner dips. For $0<U_{11}/\alpha^2<\hbar^2/m^*$ we have $E_R>E_0$ and the transmission resonance is of the $0\to 1$ type (i.e., the peak follows the dip). For $\hbar^2/m^*<U_{11}/\alpha^2<3\hbar^2/m^*$ we have $E_R<E_0$ and the resonance line shape is of the $1\to 0$ type (i.e., the location of the pole is switched with the zero energy). Thus after the value $U_{11}/\alpha^2=\hbar^2/m^*$ (where the transmission exhibits a symmetric dip) the Fano resonance is "inverted." Similar inversion of the resonance level has also been observed in Ref. 19.

The transmission coefficient T given in Eq. (35) is plotted versus the Fermi energy in Fig. 7 for progressively decreas-

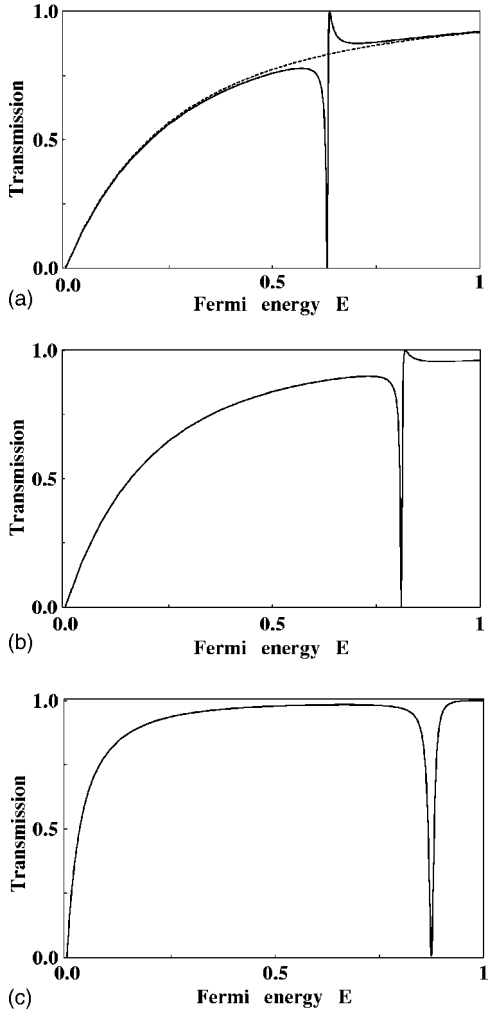

FIG. 7. Transmission coefficient T vs Fermi energy E through an attractive impurity potential $V_i(x,y)=(\hbar^2\gamma/2m^*)\mathrm{sech}^2(\alpha x)\upsilon(y)$ in a 2D quantum wire, for three values of the inverse decay length α while υ_{11} is kept fixed at the value $\upsilon_{11}=-1.5$. (a) The solid line, which corresponds to $\alpha=1.7$ with $\upsilon_{22}=-1.4$ and $\upsilon_{12}=0.08$, shows an asymmetric Fano line shape while the dashed line represents the direct transmission. (b) Corresponds to $\alpha=1.4$, $\upsilon_{22}=-0.8$, $\upsilon_{12}=0.08$ and shows a distortion of the Fano resonance. (c) Corresponds to $\alpha=1$, $\upsilon_{22}=-0.5$, $\upsilon_{12}=0.12$ and the transmission (which is generally enhanced) exhibits only a dip.

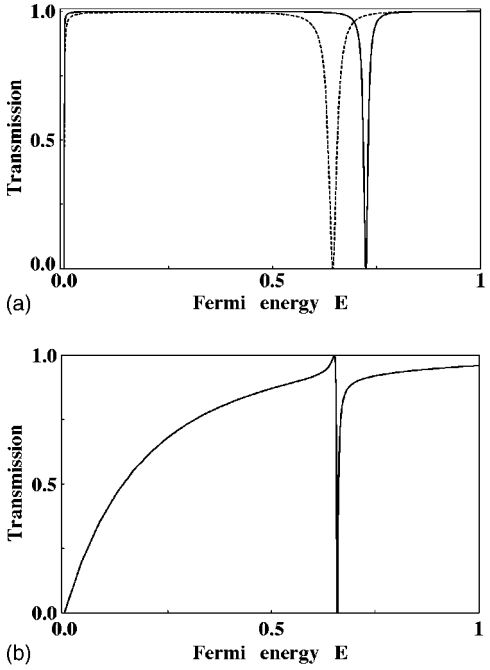

FIG. 8. Transmission coefficient T vs Fermi energy E through an attractive impurity potential $V_i(x,y)=(\hbar^2\gamma/2m^*)\mathrm{sech}^2(\alpha x)\upsilon(y)$ in a 2D quantum wire. (a) Both solid and dashed lines correspond to $\upsilon_{11}=-2$ and $\alpha=1$ so that $E_R-E_0=0$. The solid line corresponds to $\upsilon_{22}=-0.8$ and $\upsilon_{12}=0.1$ while the dashed line corresponds to $\upsilon_{22}=-0.95$ and $\upsilon_{12}=0.14$. Notice that for the larger value of $|\upsilon_{22}|$ the antiresonance moves lower in energy while its width increases (due to the larger value of υ_{12}). (b) Corresponds to appropriate values (given in the text) such that $E_R<E_0$ (i.e., the resonance level is "inverted" with respect to Fig. 7).

ing values of the inverse decay length α.[39] In Figs. 7(a)–7(c) the intrasubband matrix element υ_{11} is kept fixed to the value $\upsilon_{11}=-1.5$, while $\alpha=1.7$, 1.4, and 1, respectively. All three resonance line shapes are of the $0\rightarrow1$ type since $U_{11}/\alpha^2=0.52$, 0.77, and 1.5, respectively, which lie in the range $0<U_{11}/\alpha^2<2$ (or equivalently $0<U_{11}/\alpha^2<\hbar^2/m^*$). In Fig. 7(a) we use the values $\upsilon_{22}=-1.2$, $\upsilon_{12}=0.08$. The dashed line represents the direct (nonresonant) transmission which occurs in the decoupling limit $\upsilon_{12}=0$ (for which $\delta=\Gamma=0$). In this limit there are two scattering mechanisms: a direct (nonresonant) scattering from the first subband and a resonant scattering from the quasibound state. When the coupling to the quasibound level is nonzero the interference between direct and resonant transmission (through the quasibound state) produces the asymmetric Fano line shape, which has also been noted previously.[12,36,40]

In Fig. 7(b), where the value of the inverse decay length is smaller ($\alpha=1.4$), we note that the Fano resonance distorts while the transmission below the bound state is enhanced. In Fig. 7(b) we use the values $\upsilon_{22}=-0.8$ and $\upsilon_{12}=0.08$ in order for the transmission zero to occur closer to the bottom of the second subband so that we can make contact with the numerical results of Fig. 4(a). In Fig. 7(c) the inverse decay length has been further decreased to the value $\alpha=1$ while $\upsilon_{22}=-0.5$ and $\upsilon_{12}=0.13$. We notice that the transmission is greatly enhanced and exhibits an almost symmetric dip. As mentioned above this behavior of the transmission is due to the fact that q decreases as α decreases [which is what Eq. (36) suggests]. This is a consequence of the fact that the distance between the resonance energy and the zero energy gradually decreases leading to the progressive disappearance of the asymmetric resonance. Finally when the value of α becomes low enough such that $U_{11}/\alpha^2=2$ then $E_R=E_0$ and the transmission exhibits only a symmetric dip [as will be discussed in the context of Fig. 8(a)]. This is precisely what happens in the lower curve of Fig. 4(a) which is very similar to Fig. 7(c). However in the numerical calculations [presented in Fig. 4(a)] the strength of the intra- and intersubband coupling matrix elements could not be varied independently for the transverse δ-function potential (in fact these

matrix elements were buried inside the scattering wave function $\psi_{\mathbf{p}}^{(+)}$) and did not allow the full Fano structure to show up even for smaller values of the decay length d. Thus for large enough value of the decay length the conductance will only exhibit dips regardless of the shape of the transverse impurity potential or the values of the coupling matrix elements. To this end, we point out that if we kept the value of v_{22} fixed in Figs. 7(a)–7(c) the shape of the Fano resonance would remain exactly the same except that the transmission zero would occur at lower energies.

It was shown above that for certain values of the quantity U_{11}/α^2 the resonance energy coincides with the zero energy and in this case the transmission versus Fermi energy exhibits symmetric Breit-Wigner dips. We illustrate this result in Fig. 8(a) where both solid and dashed lines correspond to $v_{11}=-2$ and $\alpha=1$ so that $U_{11}/\alpha^2=2$. Further for the transmission represented by the solid line we used the values $v_{22}=-0.8$, $v_{12}=0.1$ while the dashed line corresponds to $v_{22}=-0.95$, $v_{12}=0.13$. The only effect of v_{22} on the transmission is to displace the location of the transmission zero. Thus increasing $|v_{22}|$ (dashed line) causes the displacement of the dip toward lower energy values. We also notice that the width of the antiresonance increases when v_{12} increases which is due to the larger coupling of the bound state with the continuum.

In Fig. 8(b) we show the transmission as a function of Fermi energy for the values $v_{11}=-5.95$, $v_{22}=-0.94$, $v_{12}=0.068$, and $\alpha=1.26$. For these values $U_{11}/\alpha^2=3.75$ and therefore the resonance line shape is of the $1\rightarrow 0$ type. The inversion of the resonance level indicates that the roles of destructive and constructive interference between the direct and resonant channels have been reversed. Thus when the spatial extension (quantified by the decay length α^{-1}) of the impurity as well as the intrasubband matrix element U_{11} have appropriate values the Fano resonance appears inverted. One could argue that by keeping the value of U_{11} fixed while continuously decreasing the value of α the quantity U_{11}/α^2 will reach the desirable values for which inversion of the Fano resonance occurs. However, it is not enough that U_{11}/α^2 be in the appropriate range. By making α very small (say $\alpha\sim 0.5$) the denominator of Eq. (36) becomes large enough so that $q\ll 1$. Consequently the transmission will exhibit a dip while the peak will hardly be discernible (due to the enhancement of the transmission).

IV. EFFECTS OF THE CROSS-SECTIONAL SHAPE ON THE CONDUCTANCE

As mentioned in the Introduction, an important issue related to electronic transport through quantum wires is how the geometry of the wires (i.e., the shape of their transverse cross section) influences the conductance. This issue has been investigated in the case of transport in 3D quantum constrictions[16,25,26,41] and in 3D rectilinear quantum wires with a δ-function impurity[23,27] and several interesting effects have been discussed. In the case of a 3D quantum wire with a δ-function impurity, the solution of the scattering problem is known to be obtainable from the characteristic discontinuity of the derivative of the propagating wave function[22,27] due to the δ function, giving rise to a phase shift. The discontinuity of the wave function depends critically on the shape of the cross section of the wire; increasing the anisotropy of the cross section leads to a progressively larger discontinuity in the derivative of the wave function resulting in a larger phase shift and increased reflection. This and other related effects (discussed in the references mentioned above) imply that the shape of the cross section can strongly affect the transport properties of a 3D quantum wire with an impurity.

Our objective in this section is to extend our previous calculations[23,27] and to investigate the influence of the cross-sectional shape of a 3D rectilinear quantum wire on the conductance through a repulsive Gaussian impurity potential of the form

$$V_i(x,y,z)=\frac{\hbar^2\gamma}{2m^*}\delta(y-y_i)\delta(z-z_i)e^{-x^2/d^2}, \tag{37}$$

where (y_i,z_i) is the impurity position along the transverse directions y and z and all other symbols have the same meaning as in the 2D case [see Eq. (8)]. The transverse position of the impurity is taken to be at $(y_i,z_i)=((5/12)w,(5/12)l)$. The cross section is chosen to be rectangular and uniform along the wire with cross-sectional area $wl=600$ nm^2, where w and l are the dimensions of the cross section along y and z. We assume an infinite square well confinement giving rise to the transverse energy levels $E_{nm}=(\hbar^2\pi^2/2m^*)[(n/w)^2+(m/l)^2]$ which define the bottoms of the subbands in the clean wire. All energies will be measured in units of E_{11}. In the scattering region the corresponding energy levels will be denoted by $E_{nm,s}$. The shape of the confining potential (defining the cross-sectional shape) is determined by the parameter s, where $s=l/w$. We will consider three different shapes corresponding to the parameter values $s=1.02$, 2.5 and 4.1. We emphasize that the strength, decay length, transverse position of the impurity, and cross-sectional area remain fixed to their initial values as s is varied. Thus the coupling of any particular transverse mode at the impurity position remains constant as the cross section is varied.

In Fig. 9(a) we show the conductance versus Fermi energy through a Gaussian impurity in a 3D quantum wire, for three different shapes of the cross section ($s=1.02$, 2.5, and 4.1). We first note that varying the cross-sectional shape causes shifting of the positions of the conductance steps and influences the character of conductance quantization. The position of a particular quantum step may shift toward higher or lower energy (depending on the cross-sectional shape anisotropy). In particular for $s=2.5$ while the first and third modes open at higher energies than the corresponding modes of the almost symmetric wire ($s=1.02$), the opening of the second mode occurs at a lower energy. However, increasing the anisotropy to $s=4.1$ forces all the conductance steps to open at higher energies. The shifting of the conductance steps originates from the rearrangement of the (transverse) electron energy levels with increasing anisotropy s as shown in Fig. 9(b). The solid lines in Fig. 9(b) denote the levels E_{nm} of the clean wire while the dashed lines denote the levels $E_{nm,s}$ in the scattering region of the wire. Note that the sec-

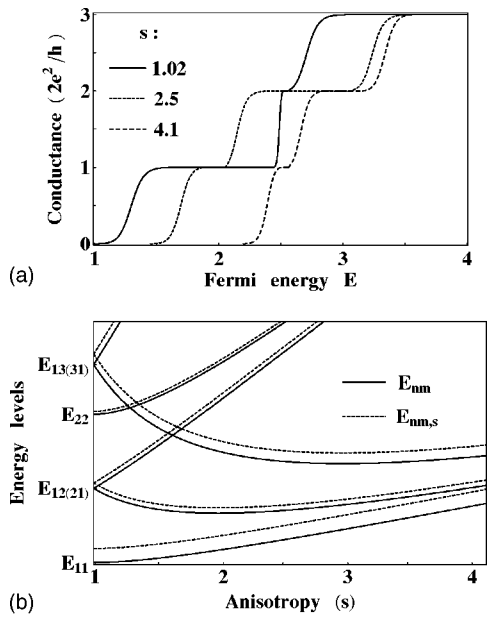

FIG. 9. (a) Conductance G (in units of $2e^2/h$) vs Fermi energy E through a Gaussian impurity of strength $\gamma=2.3$ cm^{-2} and decay length $d=20$ nm in 3D rectilinear quantum wires with asymmetric cross sections (specified by the parameter s, where $s=l/w$ and w, l are the transverse dimensions of the cross section along y and z). E is given in units of E_{11} (where E_{11} is the bottom of the first subband in the clean wire). The cross-sectional area is kept constant to the value $wl=600$ nm^2 as the shape of the cross section is varied. (b) Transverse energy levels vs the cross-sectional shape anisotropy s. Solid lines correspond to the levels E_{nm} of the unperturbed wire while the dashed lines correspond to the levels $E_{nm,s}$ in the impurity region.

ond degenerate level $E_{12(21)}$ for $s=1$ splits to two levels E_{12} and E_{21} for $s>1$. E_{12} shifts downward while E_{21} shifts upward. Similarly the fourth degenerate level $E_{13(31)}$ for $s=1$ splits to E_{13} and E_{31} which shift down and upward respectively. We also note that the distance in energy between the first E_{11} and the second E_{12} levels continuously decreases with increasing s, leading to the progressively smaller size of the plateau between the first and second steps. Further while the first level E_{11} gradually shifts upward in energy with increasing s, the second level E_{12} first shifts downward, reaches a minimum at $s=2$, and then shifts upward again. Thus at $s=2.5$ the second level is lower in energy (than the corresponding level for $s=1.02$) giving rise to the opening of the second step at lower energy (compared to the second step for $s=1.02$) as is observed in Fig. 9(a).

We also note that due to the transverse potential in the scattering region the levels $E_{nm,s}$ are slightly displaced upwards with respect to E_{nm}. However the relative distance between $E_{nm,s}$ and E_{nm} stays constant with increasing s. We also observe that the upward displacement of $E_{nm,s}$ with respect to E_{nm} is different for different levels. For example the difference $E_{12,s}-E_{12}$ is smaller than the difference $E_{11,s}-E_{11}$. This is explained in terms of the weaker coupling of the second mode (1, 2) at the impurity position (since that mode is close to have a node at the impurity) giving rise to smaller upward shifting of the subband $E_{12,s}$. Similarly the difference $E_{22,s}-E_{22}$ is slightly smaller than the difference $E_{12,s}-E_{12}$ since the coupling of mode (2, 2) at the impurity is even weaker. Placing the impurity at $(y_i,z_i)=((1/2)w,(1/2)l)$ will result to zero coupling of modes (1, 2), (2, 1), and (2, 2) at the impurity (since these modes have nodes at the impurity position). This will cause the corresponding subbands $E_{12,s}$, $E_{21,s}$, and $E_{22,s}$ in the scattering region to coincide with the subbands E_{12}, E_{21}, and E_{22} of the clean wire, for any value of s. We also note that the minimum energy of a particular mode (n,m) occurs at $s=m/n$.

When the cross section becomes almost symmetric the distance between the second and third energy levels becomes extremely small (i.e., these two levels become almost degenerate) giving rise to a plateau of a very small size [see the curve for $s=1.02$ in Fig. 9(a)]. The small size of the plateau inevitably forces the second step to rise sharply. In this case the second and third modes lie very close in energy and the second step tends to disappear. In fact for the completely symmetric wire with $s=1$, the degeneracy of the levels E_{12} and E_{21} will cause the disappearance of the second plateau and will give rise to a height of $2(2e^2/h)$ for the second conductance step. When $s=1$ the first few conductance steps have heights $1G_0$, $2G_0$, $1G_0$, $2G_0$, $2G_0$,…, where $G_0=2e^2/h$, reflecting the degeneracy of the electronic levels. Deviation from symmetry leads to splitting of the degenerate levels and restoration of the single-step (G_0) behavior of the conductance. It's also worth mentioning that under the influence of a magnetic field an otherwise symmetric cross section will become effectively asymmetric.[23,42,43] Upward or downward shifting of the (transverse) energy levels of a parabolically confined ballistic quantum wire under the influence of a longitudinal magnetic field has been observed experimentally.[43] The degenerate levels observed in Ref. 43 explain the disappearance of the corresponding plateau in the experimentally measured conductance. For specific asymmetric cross-sectional shapes there might also be accidentally degenerate levels as can be seen in Fig. 9(b). In particular the levels E_{13} and E_{22} are degenerate at $s=1.29$ for which the conductance will rise by $2G_0$ as are also the levels E_{13} and E_{21} at $s=1.631$. These degeneracies lead to occasional disappearance of steps in wires with asymmetric cross sections. Variations in the shapes of the cross section of 3D quantum point contacts have also been observed experimentally[44] in the past and such variations explain the disappearance of some of the conductance steps. Effects of this type have no analogs in 2D quantum wires.

It's also worth mentioning that examining the conductance as a function of s while keeping the Fermi energy fixed would reveal an interesting feature of the quantum transport. Namely, increasing the anisotropy of the cross section (at a fixed value of the Fermi energy) the subbands are shifted toward higher energies and therefore the contributing quantum channels decrease one by one. When the lowest subband finally crosses the fixed Fermi level, there is no open subband left and the conductance should vanish. Thus increasing s leads to depopulation of subbands (i.e., decrease in the number of conducting channels), resulting to a decrease and eventually vanishing of the conductance. This last observation suggests that cross-sectional shape anisotropy in 3D

quantum wires could be detected through conductance measurements at a fixed value of the Fermi energy.

V. SUMMARY

In this paper we have considered the transmission of electrons through a Gaussian impurity (with a decay length d along the propagation direction) in 2D and 3D rectilinear quantum wires with symmetric or asymmetric cross sections. The confining potential is that of an infinite square well. We have solved the LSE numerically and investigated several features of the conductance.

The results for the 2D wire can be summarized as follows. Increasing the decay length d of a repulsive Gaussian impurity leads to a progressively sharper rise of the conductance steps at the opening of the subbands $E_{n,s}$, as shown in Figs. 1 and 2. The physical origin of this effect is the progressively smaller contribution of tunneling modes and the gradual suppression of backscattering as the impurity potential becomes smoother.

The conductance versus the Fermi energy (for various impurity positions) was also examined. Displacing the impurity away from the central axis of the wire causes shifting of the positions of the conductance steps which is due to the corresponding displacement of the bottoms of the subbands $E_{n,s}$ in the scattering region. A particular level $E_{n,s}$ versus the impurity position follows the structure of the squared modulus of the corresponding transverse mode $|\phi_n(y)|^2$. Accordingly, depending on the particular impurity position, the coupling of a transverse mode at the impurity may be stronger or weaker leading to enhanced or suppressed scattering effects respectively (i.e., to smeared or sharp quantum steps) as shown in Fig. 3.

In the case of an attractive Gaussian impurity we have shown that there exist multiple resonance dips in the conductance which are due to the formation of quasibound states. We examined the behavior of a dip location E_{res} and the half width Γ as a function of the decay length d. We found that increasing the value of d causes shifting of E_{res} toward lower energies while the half width decays in an oscillatory manner (see Fig. 4). In particular the half width of the resonant dip may shrink to an extremely small value for some critical values of d resulting to an extremely stable state (a state with greatly enhanced lifetime).

The Feshbach approach was employed in order to analyze the scattering from a second type impurity potential (for which analytical solution to the coupled-channel equations is possible) thereby allowing us to study extensively the characteristics of the resonance line shape. The transmission was found to exhibit asymmetric Fano line shape which (for large values of the decay length) evolves into a dip while for a certain range of values of the quantity U_{11}/α^2 the Fano resonance is inverted.

We also demonstrated that the shape of the transverse cross section of a 3D wire may strongly affect the character of conductance quantization. In wires with a symmetric cross section the conductance steps have heights $2e^2/h$ or $2(2e^2/h)$, depending on the degeneracy of the transverse energy levels. In wires with asymmetric cross sections the symmetry degeneracy is removed and the single-step (height $2e^2/h$) behavior of the conductance is restored. However, accidental degeneracy may still occur for some asymmetric cross-sectional shapes. Further we demonstrated that varying the cross-sectional shape anisotropy (keeping the cross-sectional area fixed) causes shifting of the positions of the conductance steps (which is due to the rearrangement of the transverse energy levels) and changes the sizes of the plateaus between successive steps. To this end we emphasize that shape effects are important in the detailed structure of the conductance of 3D wires and effects of this type do not show up in 2D wires.

APPENDIX: CALCULATION OF THE TRANSMISSION COEFFICIENT

In this appendix we present the calculation of the transmission coefficient of the quantum wire with the impurity potential of Eq. (23) by employing the formalism of Refs. 34 and 36. For $x\to\infty$ the solution of Eq. (33) for $\psi_1(x)$ takes the form

$$\psi_1(x)=\chi_k^+(x)+\frac{m^*}{i\hbar^2kt^{bg}}\chi_k^+(x)\frac{\langle(\chi_k^-)^*|V_{12}|\Phi_0\rangle\langle\Phi_0|V_{21}|\chi_k^+\rangle}{E-E_0-\langle\Phi_0|V_{21}G_1V_{12}|\Phi_0\rangle}, \tag{A1}$$

where G_1 is the retarded Green's function which can be written in terms of the scattering states $\chi_k^{\pm}(x)$ as

$$G_1(x,x')=\frac{m^*}{i\hbar^2kt^{bg}}\times\begin{cases}\chi_k^+(x)\chi_k^-(x') & (x>x')\\ \chi_k^+(x')\chi_k^-(x) & (x<x').\end{cases} \tag{A2}$$

We will use this representation of G_1 in order to calculate the matrix elements of Eq. (A1). We then have

$$\begin{aligned}\langle(\chi_k^-)^*|V_{12}|\Phi_0\rangle&=\frac{\hbar^2}{2m^*}\gamma v_{12}\sqrt{\frac{\alpha}{2}}\int dx(e^{-ikx}+r_-^{bg}e^{ikx})\mathrm{sech}^3(\alpha x)\\&=\frac{\hbar^2}{2m^*}\gamma v_{12}\sqrt{\frac{\alpha}{2}}(I_1^*+r_-^{bg}I_1),\end{aligned} \tag{A3}$$

where

$$I_1=\int_{-\infty}^{\infty}dxe^{ikx}\,\mathrm{sech}^3(\alpha x),\quad I_1^*=\int_{-\infty}^{\infty}dxe^{-ikx}\,\mathrm{sech}^3(\alpha x). \tag{A4}$$

It turns out that $I_1=I_1^*=[(\alpha^2+k^2)\pi\,\mathrm{sech}(k\pi/2\alpha)]/2\alpha^3$. Also,

$$\langle\Phi_0|V_{21}|\chi_k^+\rangle=\frac{\hbar^2}{2m^*}\gamma v_{21}\sqrt{\frac{\alpha}{2}}t^{bg}I_1. \tag{A5}$$

For the matrix element occurring in the denominator of Eq. (A1) we have

$$\langle\Phi_0|V_{21}G_1V_{12}|\Phi_0\rangle = \frac{m^*}{i\hbar^2kt^{bg}}\int_{-\infty}^{\infty}dx\int_{-\infty}^{\infty}dx'\Phi_0(x)V_{12}(x)\Phi_0(x')V_{12}(x')\chi_k^-(x)\chi_k^+(x')$$
$$+\frac{m^*}{i\hbar^2kt^{bg}}\int_{-\infty}^{\infty}dx\int_{-\infty}^{x}dx'\Phi_0(x)V_{12}(x)\Phi_0(x')V_{12}(x')[\chi_k^+(x)\chi_k^-(x')-\chi_k^-(x)\chi_k^+(x')]$$
$$= Q_1+Q_2-Q_3. \tag{A6}$$

Inserting the explicit expressions for the bound state Φ_0, the potential V_{12} and the scattering states $\chi_k^{\pm}$ into Eq. (A6) we obtain

$$Q_1 = \frac{m^*}{i\hbar^2k}\left(\frac{\hbar^2}{2m^*}\right)^2\gamma^2\upsilon_{12}^2\left(\frac{\alpha}{2}\right)[I_1^*I_1+r_-^{bg}(I_1)^2] \tag{A7}$$

and

$$Q_2 = \frac{m^*}{i\hbar^2k}\left(\frac{\hbar^2}{2m^*}\right)^2\gamma^2\upsilon_{12}^2\left(\frac{\alpha}{2}\right)[I_2+r_-^{bg}I_3], \tag{A8}$$

where

$$I_2 = \int_{-\infty}^{\infty}dxe^{ikx}\,\mathrm{sech}^3(\alpha x)\int_{-\infty}^{x}dx'e^{-ikx'}\,\mathrm{sech}^3(\alpha x') \tag{A9}$$

and

$$I_3 = \int_{-\infty}^{\infty}dxe^{ikx}\mathrm{sech}^3(\alpha x)\int_{-\infty}^{x}dx'e^{ikx'}\,\mathrm{sech}^3(\alpha x') \tag{A10}$$

The calculation of Q_3 yields exactly the same expression as Q_2 so that $Q_2-Q_3=0$. Then $\langle\Phi_0|V_{21}G_1V_{12}|\Phi_0\rangle=Q_1$. Finally using Eqs. (A7) and the results of the integrals I_1 and I_1^* the matrix element can be written as

$$\langle\Phi_0|V_{21}G_1V_{12}|\Phi_0\rangle = \delta - i\Gamma \tag{A11}$$

with

$$\delta = -\frac{\hbar^2\gamma^2\upsilon_{12}^2(\alpha^2+k^2)^2\pi^2\,\mathrm{sech}^2(k\pi/2\alpha)}{32m^*k\alpha^5}$$
$$\times\frac{\cos[(\pi/2)\sqrt{1+(8m^*U_{11}/\hbar^2\alpha^2)}]\sinh(\pi k/\alpha)}{\sinh^2(\pi k/\alpha)+\cos^2[(\pi/2)\sqrt{1+(8m^*U_{11}/\hbar^2\alpha^2)}]} \tag{A12}$$

and

$$\Gamma = \frac{\hbar^2\gamma^2\upsilon_{12}^2(\alpha^2+k^2)^2\pi^2\,\mathrm{sech}^2(k\pi/2\alpha)}{32m^*k\alpha^5}$$
$$\times\frac{\sinh^2(\pi k/\alpha)}{\sinh^2(\pi k/\alpha)+\cos^2[(\pi/2)\sqrt{1+(8m^*U_{11}/\hbar^2\alpha^2)}]} \tag{A13}$$

giving the shift and width that the bound state acquires. Using Eqs. (A3) and (A5) the numerator of Eq. (A1) can be written also as

$$\frac{m^*}{i\hbar^2kt^{bg}}\langle(\chi_k^-)^*|V_{12}|\Phi_0\rangle\langle\Phi_0|V_{21}|\chi_k^+\rangle = \delta - i\Gamma. \tag{A14}$$

We then get for $x\to\infty$,

$$\psi_1(x) = t^{bg}e^{ikx}\frac{E-E_0}{E-E_0-\delta+i\Gamma}, \tag{A15}$$

which leads to the transmission coefficient

$$T = |t^{bg}|^2\frac{(E-E_0)^2}{(E-E_R)^2+\Gamma^2}, \tag{A16}$$

where $E_R=E_0+\delta$ and $|t^{bg}|^2$ is given as

$$|t^{bg}|^2 = \frac{\sinh^2(\pi k/\alpha)}{\sinh^2(\pi k/\alpha)+\cos^2[(\pi/2)\sqrt{1+(8m^*U_{11}/\hbar^2\alpha^2)}]}. \tag{A17}$$

*Electronic address: vargiam@physics.auth.gr

[1] B. J. van Wees, H. van Houten, C. W. J. Beenakker, J. G. Williamson, L. P. Kouwenhoven, D. van der Marel, and C. T. Foxon, Phys. Rev. Lett. **60**, 848 (1988).
[2] D. A. Wharam, T. J. Thornton, R. Newbury, M. Pepper, H. Ahmed, J. E. F. Frost, D. G. Hasko, D. C. Peacock, D. A. Ritchie, and G. A. C. Jones, J. Phys. C **21**, L209 (1988).
[3] A. Szafer and A. D. Stone, Phys. Rev. Lett. **62**, 300 (1989).
[4] D. van der Marel and E. G. Haanappel, Phys. Rev. B **39**, 7811 (1989).
[5] C. S. Chu and R. S. Sorbello, Phys. Rev. B **40**, 5941 (1989).
[6] P. F. Bagwell, Phys. Rev. B **41**, 10 354 (1990).
[7] P. F. Bagwell, J. Phys.: Condens. Matter **2**, 6179 (1990).
[8] E. Tekman and S. Ciraci, Phys. Rev. B **43**, 7145 (1991).

[9] H. Tamura and T. Ando, Phys. Rev. B **44**, 1792 (1991).
[10] A. Kumar and P. F. Bagwell, Phys. Rev. B **43**, 9012 (1991).
[11] V. Marigliano Ramaglia, F. Ventriglia, and G. P. Zucchelli, Phys. Rev. B **48**, 2445 (1993).
[12] E. Tekman and P. F. Bagwell, Phys. Rev. B **48**, 2553 (1993).
[13] H. Xu, Phys. Rev. B **48**, 8878 (1993).
[14] C. Kunze and P. F. Bagwell, Phys. Rev. B **51**, 13 410 (1995).
[15] C. Kunze, L. F. Chang, and P. F. Bagwell, Phys. Rev. B **53**, 10 171 (1996).
[16] M. Brandbyge, K. W. Jacobsen, and J. K. Norskov, Phys. Rev. B **55**, 2637 (1997).
[17] V. A. Geiler, V. A. Margulis, and L. I. Filina, Pis'ma Zh. Eksp. Teor. Fiz. **113**, 1376 (1998) [JETP **86**, 751 (1998).]
[18] E. Granot, Phys. Rev. B **60**, 10 664 (1999).
[19] C. S. Kim, A. M. Satanin, Y. S. Joe, and R. M. Cosby, Phys. Rev. B **60**, 10 962 (1999).
[20] D. Boese, M. Lischka, and L. E. Reichl, Phys. Rev. B **61**, 5632 (2000).
[21] N. G. Galkin, V. A. Geyler, and V. A. Margulis, Pis'ma Zh. Eksp. Teor. Fiz. **118**, 223 (2000) [JETP **91**, 197 (2000)].
[22] V. Vargiamidis, O. Valassiades, and D. S. Kyriakos, Phys. Status Solidi B **236**, 597 (2002).
[23] V. Vargiamidis and H. M. Polatoglou, Phys. Rev. B **67**, 245303 (2002).
[24] D. Boese, M. Lischka, and L. E. Reichl, Phys. Rev. B **62**, 16 933 (2000).
[25] A. G. Scherbakov, E. N. Bogachek, and Uzi Landman, Phys. Rev. B **53**, 4054 (1996).
[26] E. N. Bogachek, A. G. Scherbakov, and Uzi Landman, Phys. Rev. B **56**, 1065 (1997).
[27] V. Vargiamidis and O. Valassiades, J. Appl. Phys. **92**, 302 (2002).
[28] J. J. Sakurai, *Modern Quantum Mechanics* (Addison, New York, 1994), Chap. 7.
[29] P. M. Morse and H. Feshbach, *Methods of Theoretical Physics* (McGraw-Hill, New York, 1953), Vol. 1.
[30] M. Buttiker, Y. Imry, R. Landauer, and S. Pinhas, Phys. Rev. B **31**, 6207 (1985).
[31] R. Landauer, J. Phys.: Condens. Matter **1**, 8099 (1989).
[32] E. V. Sukhorukov, M. I. Lubin, C. Kunze, and Y. Levinson, Phys. Rev. B **49**, 17 191 (1994).
[33] S. Yamada and M. Yamamoto, J. Appl. Phys. **79**, 8391 (1996).
[34] S. A. Gurvitz and Y. B. Levinson, Phys. Rev. B **47**, 10 578 (1993).
[35] U. Fano, Phys. Rev. **124**, 1866 (1961).
[36] J. U. Nöckel and A. D. Stone, Phys. Rev. B **50**, 17 415 (1994).
[37] H. Feshbach, Ann. Phys. (N.Y.) **5**, 357 (1958); **19**, 287 (1962).
[38] L. D. Landau and E. M. Lifshitz, *Quantum Mechanics* (Pergamon, New York, 1965).
[39] The value of $\hbar^2/2m^*$ is 0.57 eV nm^2 for GaAs. We take $\hbar^2/2m^*$ equal to unity here. In the numerical calculations we can take the unit of the matrix elements v_{nm} to be 0.1 eV nm. This yields an energy unit of 17.7 meV and a length unit of 5.7 nm.
[40] J. U. Nöckel and A. D. Stone, Phys. Rev. B **51**, 17 219 (1995).
[41] A. G. Scherbakov, E. N. Bogachek, and Uzi Landman, Phys. Rev. B **57**, 6654 (1998).
[42] V. A. Geyler and V. A. Margulis, Phys. Rev. B **61**, 1716 (2000).
[43] G. Salis, T. Heinzel, K. Ensslin, O. J. Homan, W. Bachtold, K. Maranowski, and C. Gossard, Phys. Rev. B **60**, 7756 (1999).
[44] J. I. Pascual, J. Mendez, J. Gomez-Herrero, A. M. Baro, N. Garcia, U. Landman, W. D. Luedtke, E. N. Bogachek, and H.-P. Cheng, Science **267**, 1793 (1995).